Scaling Rules for Resonance Dynamics near a Saddle Point: The Pendulum as a Zero-Order Model[†]

Matthew P. Jacobson[‡] and Mark S. Child*

Physical and Theoretical Chemistry Laboratory, Oxford University, South Parks Road, Oxford OX1 3QZ, U.K.

Received: December 14, 2000

The pendulum is the simplest zero-order model for an isomerizing vibrational mode (one which passes through a saddle point). We utilize the classical action/angle theory of the pendulum, for which new results are given in the appendix, to determine generic scaling laws between the quantum mechanical pendulum eigenvalue distribution and the coupling matrix elements. These scaling rules are more appropriate for isomerizing vibrational modes than are the usual harmonic oscillator scaling rules, encoded in traditional spectroscopic effective Hamiltonians, which break down catastrophically at a saddle point. As a simple example of resonant quantum dynamics in the vicinity of a saddle point, we analyze a system consisting of a pendulum model for bend/internal rotor motion, anharmonically coupled to a stretching harmonic oscillator, in qualitative agreement with the known dynamics of HCP. The dominance of just two of the infinite number of resonances, 2:1 and 4:1, at all energies including that of the saddle point, is related to the scaling properties of the zero-order pendulum model.

I. Introduction

The most common effective Hamiltonian models for molecular vibrations are expressed in terms of harmonic oscillator shift operators for the various (normal or local mode) vibrational degrees of freedom. That is, the harmonic oscillator is taken as the zero-order model, and anharmonicities are accounted for by (1) Dunham-type expansions for the zero-order energies (diagonal matrix elements) and (2) various anharmonic vibrational resonances, also expressed in terms of the shift operators, which couple the vibrational modes. In practice, such effective Hamiltonian models are usually derived by one of two methods. If a potential energy surface of sufficient accuracy is available, then perturbation theory (a series of successive unitary transformations) can be used to derive a (generally high order) effective Hamiltonian from the surface (e.g., refs 1 and 2). More commonly, the parameters are fitted directly to experimental or theoretical data. In this case, the parameters cannot be rigorously related to terms in the potential surface (i.e., they have no simple physical interpretation by themselves, although together they have predictive power), and, importantly in the context of this paper, the parameters included in the model are generally chosen without regard to consistency between the zeroth-order (diagonal) and coupling (off-diagonal) constants.

The harmonic oscillator is not the only possible choice of the zero-order model. Efforts have been made to derive effective Hamiltonian models, based on Lie algebras, which implicitly use the Morse oscillator as a zero-order model (see, e.g., refs 3−6). These models, at least for certain molecules/vibrational modes, are more quickly convergent; that is, they can, in principle, provide more compact, physical models. In practical application, the primary difference between traditional effective

Hamiltonians and those based on, e.g., SU(2) algebras, is the precise scaling of the matrix elements. In an anharmonic algebraic model, there is still a Dunham-like expansion (in Casimir operators) for the diagonal matrix elements, but the lowest order terms implicitly include effects of anharmonicity which are only accounted for at higher order in models based on the harmonic oscillator. Similar differences also occur in the scaling of the off-diagonal matrix elements; that is, the scaling of the off-diagonal matrix elements is also dictated by the underlying vibron model consistent with the SU(2) algebra.

Neither the harmonic oscillator nor the Morse oscillator provides an adequate zero-order model for vibrational dynamics in the vicinity of a saddle point. Effective Hamiltonian models based on harmonic or anharmonic oscillators can, of course, successfully reproduce vibrational energetics/dynamics below a saddle point, and even above for those states which have negligible isomerizing character.[7,8] However, as explored here and in previous publications,[9,10] these models fail catastrophically for vibrational dynamics/eigenstates that probe the vicinity of a saddle point. This paper focuses on the scaling of off-diagonal matrix elements in systems with a saddle point, which we demonstrate cannot be adequately reproduced, in a global sense, by effective Hamiltonian models based on harmonic or anharmonic oscillators. This breakdown is most evident at energies near or above that of the saddle point, but harmonically coupled anharmonic oscillator models (the most common form for effective Hamiltonians) are also demonstrated to be inadequate well below the saddle-point energy.

The focal point of this paper is a derivation of the scaling rules that are appropriate for a zero-order pendulum model, i.e., for motion in a simple sinusoidal potential $V(1 - \cos \theta)$. This is one of the simplest models to explicitly include a local maximum and is particularly relevant to systems which can undergo bond-breaking internal rotation,[9,10] such as HCP−HPC[11] or acetylene−vinylidene.[7] The pendulum is also an attractive zero-order model because its scaling rules can be

Scaling Rules for Resonance Dynamics

J. Phys. Chem. A, Vol. 105, No. 12, 2001 **2835**

expressed analytically, as demonstrated in the appendix. We say zero order because, just as no bond stretch in a real molecule is perfectly represented by a harmonic or even a Morse oscillator, neither is any real bond-breaking internal rotation, even in small molecules with simple potential surface topologies such as HCP,[11] adequately represented by a simple pendulum. Our emphasis, however, is on generic features of the scaling rules of systems with saddle points and the limitations of harmonic oscillator-based models for representing these systems. Furthermore, the approach we take, being based on fundamental principles of semiclassical mechanics, is general, and it will be clear that the precise scaling rules for more complicated systems can be derived in a similar manner (one possible approach is to represent more complicated isomerization potentials as superpositions of simple pendula).

We wish to note briefly that, although we focus on isomerizing systems, the scaling rules derived are also applicable to non-bond-breaking internal rotations, such as those of methyl groups. We do not anticipate that the results will be as useful in that context, however, because of the small number of quantum levels with energies below the barrier to internal rotation. On the other hand, for bond-breaking internal rotor systems, the number of vibrational quantum states below the saddle point will generally be quite large, and a primary experimental and theoretical challenge is the detection of signatures of the isomerization within complex, congested spectra. This paper lays the groundwork for the development of effective Hamiltonian models that are appropriate to describe spectroscopic patterns marking the transition from purely vibrational motion to hindered internal rotation.

II. Action/Angle Representation of the Pendulum

The pendulum is amenable to an exact transformation to action/angle variables, from which, using standard principles of quantum-classical correspondence, various scaling properties may be deduced, both for the eigenvalue spectrum and for the coupling matrix elements. Mathematical details are given in the appendix. Certain portions of this derivation are familiar and are repeated for completeness; however, the expressions for Fourier components in classical angle variables, which dictate the quantum off-diagonal matrix element scaling, are not readily available elsewhere.

The results in the appendix apply to the spherical pendulum, which is free to rotate on the surface of a sphere under the classical Hamiltonian

$$H = \frac{1}{2I}\left(p_\theta^2 + \frac{p_\phi^2}{\sin^2\theta}\right) + B\sin^2\frac{\theta}{2} \quad (1)$$

where p_ϕ is the angular momentum about the z axis, I is a moment of inertia, and B is the maximal potential energy. Here in the main text we restrict our attention to the special case of $p_\phi = 0$, for which the pendulum swings in a plane, but details of the angle/action theory differ little with p_ϕ. Moreover, the general case is relevant to isomerization-type motions in, for example, HCP and acetylene, which contain doubly degenerate bending vibrational modes that play a critical role in the isomerization dynamics of each molecule. In such systems, there is an additional scaling of the matrix elements with the value of the vibrational angular momentum p_ϕ, the form of which can readily be deduced from the results in the appendix, but we do not discuss this scaling further.

Turning to the planar case, the action, which is the classical equivalent of a quantum number, is defined as

$$J = \frac{1}{2\pi}\oint p_\theta \, d\theta = \frac{1}{\pi}\int_{\theta_1}^{\theta_2}\sqrt{I[2E - B(1 - \cos\theta)]} \, d\theta \quad (2)$$

where θ_1 and θ_2 are the classical turning points. It is readily verified that the correspondence

$$J_v = (v + 1)\hbar \quad (3)$$

between action and quantum number for a doubly degenerate oscillator leads to a scaling law between the quantum number and the reduced energy $\epsilon = E/B$ (see eqs A42 and A51)

$$\frac{(v + 1)\hbar}{\sqrt{2IB}} = f(\epsilon) \quad (4)$$

The precise functional form of $f(\epsilon)$ need not concern this discussion, but it is monotonic and expressed in terms of elliptic integrals. Conversely, the reduced energy levels may be expressed as

$$\epsilon_v = \frac{E_v}{B} = h\left[\frac{(v + 1)\hbar}{\sqrt{2IB}}\right] \quad (5)$$

where h is the inverse function to $f(\epsilon)$. It also follows by differentiation of eq 4 that the local quantum level separation may be approximated in terms of the local classical frequency in the form

$$\frac{1}{2}(E_{v+1} - E_{v-1}) \simeq \hbar\omega_v(\epsilon) = \hbar\sqrt{\frac{B}{2I}}[f'(\epsilon)]^{-1} \quad (6)$$

The shape of this classical frequency profile, with its characteristic "Dixon dip"[12] in Figure 1a, is central to the resonance discussion. The agreement between the classical curve and dots marking the quantum level separations (using the parameters defined in section III) confirms the accuracy of the correspondence implied by eq 6, with the important proviso that the classical frequency falls to zero at $E = B$, whereas the quantum level spacing remains finite. The semiclassical theory of such barrier-related corrections may be found in section 3.3 of the text by Child.[13]

Next, the Heisenberg correspondence between matrix elements and classical Fourier components[14] can be used to assess the magnitude and energy dependence of the coupling strength at different orders. To take a familiar example, the semiclassical equivalent of the harmonic oscillator creation operator is given by[13]

$$a^\dagger = \frac{1}{\sqrt{2}}(q - ip) = \sqrt{v + \frac{1}{2}}e^{i\alpha} \quad (7)$$

where α is the relevant classical angle variable. The generic form of the semiclassical wave function

$$\psi_v = \frac{1}{\sqrt{2\pi}}e^{iv\alpha} \quad (8)$$

therefore implies that

$$\langle v'|a^\dagger|v\rangle = \frac{1}{2\pi}\int_0^{2\pi}\sqrt{\bar{v} + \frac{1}{2}}e^{i(v - v' + 1)\alpha} \, d\alpha = \sqrt{v + 1}\delta_{v',v+1} \quad (9)$$

after evaluating $\bar{v}$ as the average of v and $v + 1$.

The same idea transfers to the present more complicated problem, although, because θ is a cyclic variable, it is most
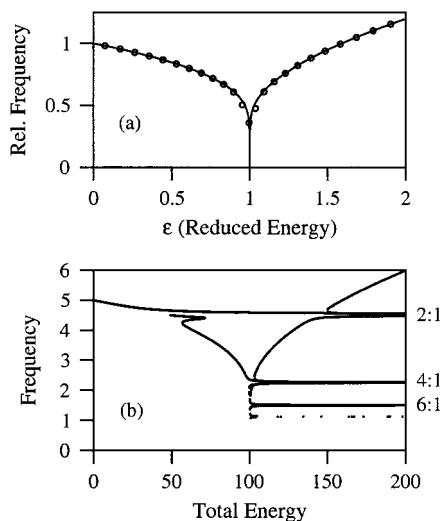
Figure 1. (a) Classical frequency and quantum energy level spacings for the zero-order pendulum model. The *y* values are scaled such that the classical frequency approaches 1.0 as $\epsilon \rightarrow 0$. The quantum energy levels are calculated using the parameters defined in section III. (b) Bifurcation diagram illustrating the frequencies of periodic orbits of the system defined in eqs 12–15. Resonances occur as the pendulum frequency passes through integer ratios with the fixed stretch frequency, $\hbar\omega_s = 9$.

appropriate to express the quantities of interest in terms of trigonometric functions of θ. For example, it is shown in the appendix that

$$\sin^2\theta = \sum_{\mu=0}^{\infty} C_{2\mu}(\epsilon)\cos 2\mu\alpha \qquad (10)$$

where ϵ is the reduced energy and expressions for the coefficients $C_{2\mu}(\epsilon)$ (once again expressed in terms of elliptic integrals) are given by eqs A30–A36. It follows that

$$\langle v + \mu|\sin^2\theta|v - \mu\rangle = \frac{1}{2}(1 + \delta_{\mu 0})C_{2\mu}(\epsilon_v) \qquad (11)$$

Comparison between the dots and solid lines in Figure 2 demonstrates the remarkable accuracy of the above correspondence, apart from some minor discrepancies in the immediate vicinity of $\epsilon = 1$. Not only are the relative magnitudes of different types of matrix elements clearly displayed but the classical curves are also universal functions of the reduced energy, applicable to any pendulum Hamiltonian. Different parameter sets B and I simply determine the positions of the quantum mechanical reduced energy levels ϵ_v. Thus, eq 11 provides an example of the scaling associated with matrix elements of the pendulum eigenstates; expressions for matrix elements involving other trigonometric functions of θ can also be derived. The dashed lines, which follow power series of different orders for the C_2 coefficients, will be discussed at the end of section III, in the context of the limitations of effective Hamiltonian models for reproducing the pendulum scaling rules. For now, we note simply that no power series can reproduce the cusplike changes around $\epsilon = 1$.

III. Pendulum-Based Scaling Rules in Practice: A Simple Example

To provide a practical demonstration of how the results in section II can be used to dictate the scaling rules for a quantum mechanical effective Hamiltonian, we consider in this section
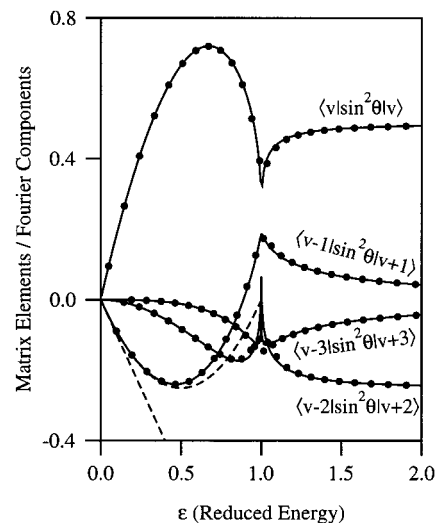

Figure 2. Planar pendulum scaling rules for classical or quantum resonances. The solid lines are the C_n's obtained from Fourier expansion of the classical angles. The dots are the corresponding quantum matrix elements. The dashed lines indicate linear and quadratic series expansions for the C_2 coefficients. The linear approximation, which would be encoded in a harmonically coupled anharmonic oscillator model, is totally inadequate, while the quadratic approximation is reasonable for $\epsilon < 0.75$. However, no series expansion can represent the cusps at $\epsilon = 1$.

a model Hamiltonian of the form

$$H = H_s + H_b + H_{int} \qquad (12)$$

$$H_s = \frac{\hbar\omega_s}{2}(p_s^2 + q_s^2) \qquad (13)$$

$$H_b = -\frac{\hbar^2}{2I}\frac{d^2}{d\theta^2} + B\sin^2\frac{\theta}{2} \qquad (14)$$

$$H_{int} = V'q_s\sin^2\theta \qquad (15)$$

This Hamiltonian represents a pendulum which is periodically "kicked" by coupling to a harmonic oscillator. Such systems have been widely studied in the context of classical chaos;[15,16] our central concern is the scaling of the Hamiltonian matrix elements and the relationship of this scaling to vibrational dynamics, including classical chaos. This Hamiltonian differs from a conventional resonance Hamiltonian by inclusion of the "pendulum" term designed to produce a saddle point at $\theta = \pi$. Second, the coupling term employs a properly periodic trigonometric term in place of the more usual combinations of harmonic oscillator creation and annihilation operators.

To provide a concrete example of the relevance of this Hamiltonian to molecular systems, HCP has a saddle point on its ground electronic state surface at the linear configuration CPH ($\theta = \pi$) with an energy of roughly $B = 27\,000$ cm^{-1}. The bend mode v_2 at energies $E > B$ becomes a hindered internal rotor mode in which the hydrogen "orbits" around the CP core, breaking/forming bonds to C and P in the process. Thus, we label the pendulum mode in our model b for "bending", although this is only an appropriate label at $E < B$. The harmonic oscillator mode in the model, s, would in this context represent the CP stretch in HCP, which is strongly coupled to the bend/internal rotor mode. Although HCP inspired this model, no effort is made to model the behavior of any particular molecule. For the purposes of illustration, the following parameter values (expressed in scaled energy units) will be employed: $B = 100$,

Scaling Rules for Resonance Dynamics

J. Phys. Chem. A, Vol. 105, No. 12, 2001 **2837**

$\hbar\omega_s = 9$, $\hbar^2/2I = 0.5$, and $V' = -3$. These parameters lead to a small-amplitude bending quantum, $\hbar\omega_b = 5$, which is slightly larger than half the stretching quantum, $\hbar\omega_s = 9$, and to a bending quantum number of roughly 25 at the barrier maximum.

The simplicity of the model allows ready diagonalization in a harmonic oscillator (stretch), spherical harmonic (bend/internal rotor) product basis set. However, we have carried out these "exact" quantum calculations primarily to validate our other results, because we have demonstrated in section II that analytical scaling rules reproduce with excellent precision the relevant matrix elements in a product basis set that employs the pendulum eigenstates for the bend/internal rotor mode. The classical mechanics can readily be solved by integrating Newton's equations of motion (in either the position/momentum or action/angle representations), and periodic orbits, as well as classical chaos, can be identified with the aid of surfaces of the section in ref 9.

As can be seen in Figure 1a, the pendulum frequency tunes downward through integral fractions of the stretching frequency as $\epsilon \rightarrow 1$ and then upward through the same resonance conditions at higher energies, an important feature that is underlined by the classical periodic orbit bifurcation diagram shown in Figure 1b. This latter diagram, taken from an earlier fully coupled classical study of the same model,[9] clearly shows the sequential onset and persistence of 2:1, 4:1, and 6:1 resonances as the energy increases, although there are an infinite number of resonances (which cannot be fully depicted on the diagram) at $E > B$. However, the 2:1 resonance dominates the dynamics until the energy almost reaches the saddle point, for two reasons. First, the scaling of the zero-order pendulum frequency is such that it decreases relatively slowly and quasi-linearly at energies up to $\epsilon \approx 0.75$ and thus remains in a nearly 2:1 frequency ratio with the stretch. Second, as can be seen in Figure 2, the magnitude of the 2:1 resonance strength is predicted to be larger than that of any other resonance up to $\epsilon \approx 0.75$.

At energies where the single (2:1) resonance approximation holds, an approximately conserved *polyad* quantum number[17,18] can be defined as $N_p = v_b + 2v_s$; this type of approximation is well established for HCP and many other small molecules. The breakdown of this approximation, considered in detail elsewhere[9] and in summary here, is less well understood but is very closely related to the scaling rules under consideration. The breakdown in the single-resonance approximation occurs rapidly as $E \rightarrow B$, again for two reasons. First, the pendulum frequency begins to drop increasingly quickly. Second, the strength of the 2:1 resonance passes through zero, at roughly the same bend energy ($\epsilon \approx 0.8$) at which the 4:1 resonance strength passes through a maximum. Moreover, the 4:1 resonance cannot be ignored at any higher energy, particularly because the $\langle v_b + 2|\sin^2\theta|v_b - 2\rangle$ matrix element in Figure 2 remains finite at all $\epsilon > 1$.

The importance of the higher order resonances is less clear. The scaling rules illustrated in Figure 2 suggest that the strength of these high-order resonances, except at bend energies very near that of the saddle point, are substantially less than those of the 2:1 and 4:1 resonances. In addition, comparison between parts a and b of Figure 1 shows that the minimum quantum level spacing is well above the 6:1 energy quantum, $\Delta E = \hbar\omega_s/6 = 1.5$.

To quantitatively assess these predictions, we investigate single- and multiple-resonance approximations to the full Hamiltonian, which contains an, in principle, infinite number of resonances. The simplest reduction of the model Hamiltonian
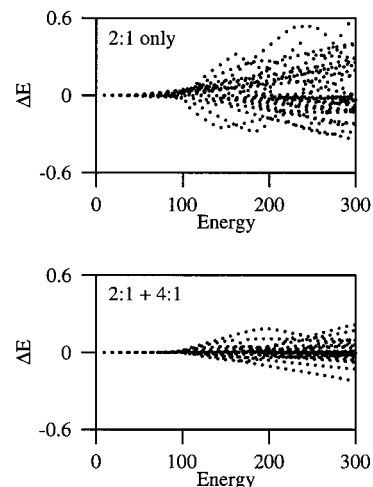

Figure 3. (Upper) Energy errors resulting from including only the 2:1 matrix elements in the quantum Hamiltonian. (Lower) Same as the upper panel, except that both 4:1 and 2:1 matrix elements are retained.

to the 2μ:1 resonance form (μ is a positive integer) would involve diagonalization in the product basis $|v_s\rangle|v_b\rangle$ such that

$$(H_s + H_b)|v_s\rangle|v_b\rangle = \left[\left(v_s + \frac{1}{2}\right)\hbar\omega_s + E_{v_b}\right]|v_s\rangle|v_b\rangle \quad (16)$$

subject to the polyad constraint

$$N_p = 2\mu v_s + v_b = \text{constant} \quad (17)$$

Greater accuracy can, however, be obtained by including the relatively large diagonal matrix elements $\langle v_b|\sin^2\theta|v_b\rangle$ in the zeroth-order Hamiltonian, because the mean Hamiltonian in a given pendulum state $|v_b\rangle$ reduces to the displaced harmonic oscillator form

$$\langle v_b|H|v_b\rangle = E_{v_b} + \frac{\hbar\omega_s}{2}\{p_s^2 + [q_s + q^0(v_b)]^2\} - \frac{\hbar\omega_s}{2}q^0(v_b)^2 \quad (18)$$

where

$$q^0(v_b) = \frac{V'\langle v_b|\sin^2\theta|v_b\rangle}{\hbar\omega_s} \quad (19)$$

The eigenfunctions of $\langle v_b|H|v_b\rangle$ are, therefore, parametrically dependent on v_b

$$\langle q_s|v_s; v_b\rangle = \psi_{v_s}[q_s + q^0(v_b)] \quad (20)$$

where $\psi_{v_s}(q_s)$ is the scaled harmonic oscillator function. The diagonal matrix elements of the resonance Hamiltonian are, therefore, given by

$$\langle v_s, v_b|H_{res}|v_s, v_b\rangle = \left(v_s + \frac{1}{2}\right)\hbar\omega_s + E_{v_b} - \frac{\hbar\omega_s}{2}q^0(v_b)^2 \quad (21)$$

while the off-diagonal terms are given by

$$\langle v_s - 1, v_b + \mu|H_{res}|v_s, v_b - \mu\rangle =$$
$$V'\langle v_s - 1; v_b + \mu|q_s|v_s; v_b - \mu\rangle\langle v_b + \mu|\sin^2\theta|v_b - \mu\rangle \quad (22)$$

in which the q_s matrix element is taken between displaced harmonic oscillator functions. The upper panel of Figure 3 show the discrepancies between the lowest 591 converged eigenvalues

of the full model (all of those with $E < 3B$) and those derived from the 2:1 resonance Hamiltonian of eqs 21 and 22. It is evident that inclusion of the single 2:1 resonance accurately reproduces the spectrum at energies in the range $E < B = 100$; the root-mean-square (rms) error of the 67 levels in this range is 0.014. The level of agreement for $E > B = 100$ is, however, markedly inferior; the rms error of all states on the plot is 0.15. This observation is consistent with the discussion around Figure 1, which shows that the single 2:1 resonance strongly dominates at $\epsilon < 1$ but that the 4:1 resonance is nonnegligible at all energies with $\epsilon > 1$. The lower panel shows that the inclusion of both the 2:1 and 4:1 resonance terms removes a large fraction of the remaining errors. As many as 91% of the total of 591 eigenvalues below $E = 3B$ are now reproduced with an error of less than 0.1. The remaining errors, which are generally quite small but increase with increasing energy, are accounted for collectively by the 6:1 and higher order resonances. The overall picture that arises is that the 2:1 resonance dominates at all energies, but the 4:1 resonance cannot be ignored at energies near and above that of the saddle point; higher order resonances play a relatively minor role.

We note in passing that the presence of multiple (here primarily two) interacting resonances at energies above the saddle point is essential for any theory of "isomerization" between bending states with exponentially low amplitudes at the saddle point and rotating states that circle through it. At least in a classical sense, the validity of a single-resonance model restricts the classical dynamics to regular motion in a two-dimensional phase space, in which case the isomerization could occur only by dynamical tunneling. The simultaneous action of two or more resonances is essential for RRKM-like chaotic energy transfer between the two types of motion. Work is in hand to assess such effects within the present 2:1 plus 4:1 coupling model.

We wish to conclude this section with a brief discussion of the extent to which our model system, and real molecular isomerizing systems, can be represented by traditional harmonic oscillator effective Hamiltonian models. That is, although the scaling rules that we have derived for the pendulum are, by design, exact for the model Hamiltonian, real molecular systems with saddle points have been adequately described by traditional effective Hamiltonian models with polyad quantum numbers, at energies below and even above that of the saddle point (e.g., in acetylene[8,7]). The first critical point is that the key parameter for the breakdown of polyad effective Hamiltonians for describing systems with saddle points is not the total energy but the amount of energy in the isomerizing mode. That is, as discussed in detail in ref 9, states with vibrational excitation primarily in modes orthogonal to the isomerizing mode can continue to be adequately described by harmonic oscillator models, even at energies far above the saddle point.

The second critical point is that effective Hamiltonian models, in addition to incorporating only the most important of the generally infinite number of resonances (which we have shown above is appropriate for most states of the model system at all energies), represent *polynomial approximations* to the proper scaling rules, such as those which we have derived for the pendulum. The standard Dunham-type, polynomial expansion in the vibrational quanta provides a flexible parametrization for the diagonal matrix elements of the effective Hamiltonian. However, such an expansion is, of course, fundamentally incapable of reproducing the Dixon dip in the frequency of pendulum-like modes. A sufficiently high order Dunham expansion can reproduce the frequency of the pendulum below

the saddle point, but the frequency associated with the polynomial expansion will diverge to positive or negative infinity as $\epsilon \rightarrow 1$, as the high-order terms begin to dominate.[10]

A similar situation holds for the off-diagonal matrix elements. The "cusps" in the magnitude of the matrix elements at $\epsilon = 1$ (Figure 2) clearly cannot be accommodated by a polynomial expansion. Moreover, the nonlinearity of the resonance strength at $E < B$ is often neglected entirely, as in the common "harmonically coupled anharmonic oscillator" models (even when nonlinearity is included, consistency between the scaling of the resonance strength and the zero-order energies is seldom considered). To take a concrete example, the 2:1 resonance matrix elements in our model are scaled according to

$$\langle v_s - 1, v_b + 1|q_s \sin^2 \theta|v_s, v_b - 1\rangle \propto \sqrt{v_s}C_2(\epsilon_{v_b}) \quad (23)$$

with the form of C_2 shown in Figure 2. By contrast, the simplest parametrization of the 2:1 resonance in a harmonic oscillator effective Hamiltonian would be

$$\langle v_s - 1, v_b + 1|\hat{a}_s\hat{a}_b^\dagger\hat{a}_b^\dagger|v_s, v_b - 1\rangle \propto \sqrt{v_s v_b(v_b + 1)} \quad (24)$$

In other words, the 2:1 resonance in the harmonic approximation scales linearly with the quantum number v_b, whereas the pendulum scaling is highly nonlinear, even at $\epsilon < 0.5$. The nonlinearity can be partially reproduced in the effective Hamiltonian by a more complex scaling of the form $1 + \beta_1 v_b + \beta_2 v_b^2 + ...)\sqrt{v_s v_b(v_b+1)}$ (that is, by introducing an expansion in the number operators for the vibrational modes). However, any type of series expansion, such as those represented by the dashed lines in Figure 2 (see eq A46), will break down in the same manner as the Dunham expansion, as $\epsilon \rightarrow 1$. In contrast, we believe that the use of pendulum-based scaling rules can help to ensure consistency between the diagonal and off-diagonal matrix elements in systems with saddle points and permit the description of states with "isomerization character" within an effective Hamiltonian framework. Comments on the practical application of this method are provided in the discussion below.

IV. Discussion

We turn now to the implications of these results for the interpretation of molecular spectra, at energies near and above a saddle point, or indeed for analysis of the accurate quantum dynamics on ab initio potential energy surfaces. The present model itself is clearly oversimplified for any specific application, but it does point to the advantages of identifying an accurate zeroth-order part of any effective spectroscopic Hamiltonian, so that the dependence of the coupling terms on the energy or quantum number can be properly related to the appropriate zeroth-order states. One approach that we have explored elsewhere[10] is to combine information from the diagonal parts of a conventional low-energy effective Hamiltonian, with ab initio information on the saddle-point region to produce a more realistic bending/rotating Hamiltonian form; a variant of the diatomic molecule RKR method[13] proved useful in this context. The relevant zeroth-order states can be obtained quantum mechanically, and the fitting problem reduces to determination of the coupling functions or operators and possibly the coordinate dependence of effective masses in the system.[10]

Another approach is to recognize that the pendulum model embodies the essential physics of the problem but to realize that the zeroth-order bending/rotating eigenvalues will not precisely follow the form in eq 4, with $f(\epsilon)$ derived from eqs A42 and A51. One might, however, assume that the reduced

Scaling Rules for Resonance Dynamics

J. Phys. Chem. A, Vol. 105, No. 12, 2001 **2839**

energy scaling between the level spacing distribution $\hbar\omega_b(\epsilon)$ and the Fourier components $C_{2\mu}(\epsilon)$ remains approximately valid. The fitting problem would then reduce to estimation of the barrier height B and the modified pendulum eigenvalue distribution E_{v_b}. The predicted existence of a single dominant resonance at energies below the saddle point suggests that a 2:1 polyad analysis would yield information that could be extrapolated to higher energies, by either of the above techniques.

Appendix: Angle/Action Variables for the Spherical Pendulum

Some relatively familiar material[15] is repeated for completeness, but the Fourier series for $\sin^2\theta$ in terms of the classical angle variable are not readily available elsewhere.

A.1. Classical Actions and Frequency. The action variables for the spherical pendulum Hamiltonian

$$H = \frac{1}{2I}\left(p_\theta^2 + \frac{p_\phi^2}{\sin^2\theta}\right) + B\sin^2\frac{\theta}{2} \tag{A1}$$

are given, together with their quantum number equivalents, by

$$J_\phi = m\hbar = \frac{1}{2\pi}\oint p_\phi\,\mathrm{d}\phi = p_\phi \tag{A2}$$

$$J_\theta = \left(n_\theta + \frac{1}{2}\right)\hbar = \frac{1}{2\pi}\oint p_\theta\,\mathrm{d}\theta =$$

$$\frac{1}{\pi}\int_{\theta_1}^{\theta_2}\frac{\sqrt{2I\left(E - B\sin^2\frac{\theta}{2}\right)\sin^2\theta - m^2\hbar^2}}{\sin\theta}\,\mathrm{d}\theta \tag{A3}$$

where θ_1 and θ_2 are the classical turning points. For reasons of space, results are restricted to $J_\phi = m\hbar = 0$ and reference to J_ϕ and m will be suppressed, but the method of derivation is readily extended to nonzero m.

Equations A2 and A3 determine the action for the individual θ and ϕ motions, but it is convenient, for comparison with standard vibrational theory, to employ the composite action

$$J_v = (v + 1)\hbar = 2J_\theta + |J_\phi| \tag{A4}$$

in place of J_θ, in which case v reduces to the degenerate harmonic oscillator quantum number in the limit $E \ll B$, for which small-angle approximations are appropriate in eq A1.

Returning to the classical theory, eqs A2−A4 imply an angle/action Hamiltonian of the form

$$E = H(J_v) \tag{A5}$$

with frequency

$$\omega_v = \partial H/\partial J_v \tag{A6}$$

The manipulations that follow are conveniently simplified by introduction of the dimensionless quantities

$$a = \frac{2E}{B} - 1 \qquad b^2 = \frac{\hbar^2}{IB} \tag{A7}$$

It is also convenient to define

$$z = \cos\theta \tag{A8}$$

$$(a + z)(1 - z^2) = (z_1 - z)(z - z_2)(z - z_3) \tag{A9}$$

$$c = \frac{2}{\sqrt{z_1 - z_3}} \tag{A10}$$

where the roots z_i are ordered as $z_1 > z_2 > z_3$.

One then finds by the use of standard tables[19,20] that

$$v + 1 = \frac{2}{\pi b}\int_{z_2}^{z_1}\frac{(a + z)\,\mathrm{d}z}{\sqrt{(z_1 - z)(z - z_2)(z - z_3)}}$$

$$= \frac{2c}{\pi b}[(z_1 - z_3)E(k) + (a + z_3)K(k)] \tag{A11}$$

while the inverse of the quantum level spacing is given by

$$\left(\frac{\partial v}{\partial E}\right)_m = \frac{1}{\hbar\omega_v} = \frac{2}{\pi}\sqrt{\frac{I}{B}}\int_{z_2}^{z_1}\frac{\mathrm{d}z}{\sqrt{(z_1 - z)(z - z_2)(z - z_3)}} =$$

$$\frac{2c}{\pi}\sqrt{\frac{I}{B}}K(k) \tag{A12}$$

The functions $K(k)$ and $E(k)$ in these expressions are complete elliptic integrals of the first and second kinds, respectively, with argument

$$k^2 = \frac{z_1 - z_2}{z_1 - z_3} \tag{A13}$$

Thus, the ordering convention $z_1 > z_2 > z_3$ restricts k to the range $0 \leq k \leq 1$. Readers should note that Abramowitz and Stegun[21] employ a variable m in place of the present k^2.

The convenience of this formulation is that eqs A11−A13 apply at all energies, although the following change in the root positions

$$(z_1, z_2, z_3) = (1, -a, -1) \qquad E < B$$

$$= (1, -1, -a) \qquad E > B \tag{A14}$$

alters the physical significance of the results, which are explored in section A.3. Moreover, extension to nonzero values of m involves two relatively minor changes. An additional term in eq A9 shifts the position of the roots, and a further term (expressible in terms of elliptic integrals of the third kind) appears in eq A11.

A.2. Classical Angle and Fourier Components. Turning from action to angle, the conjugate variable to J_v is given by the partial derivative of the generating function[13,22]

$$S(J_v, J_\phi) = \int_{\theta_1}^{\theta}p[H(J_v, J_\phi), J_\phi, \theta]\,\mathrm{d}\theta + \int_0^\phi J_\phi\,\mathrm{d}\phi \tag{A15}$$

Thus, following the notation of Child[13] to avoid confusion with the spherical polar variables

2840 *J. Phys. Chem. A, Vol. 105, No. 12, 2001*

Jacobson and Child

$$\alpha_v = \frac{\partial S}{\partial J_v} = \sqrt{\frac{I}{B}\left(\frac{\partial H}{\partial J_v}\right)} \int_{\theta_1}^{\theta} \frac{\sin\theta \, d\theta}{\sqrt{(a + \cos\theta)\sin^2\theta - m^2 b^2}}$$

$$= \sqrt{\frac{I}{B}\left(\frac{\partial H}{\partial J_v}\right)} \int_z^{z_1} \frac{dz}{\sqrt{(z_1 - z)(z - z_2)(z - z_3)}}$$

$$= \sqrt{\frac{I}{B}\left(\frac{\partial H}{\partial J_v}\right)} cF(\psi, k) \qquad (A16)$$

where

$$\sin^2\psi = \frac{z_1 - z}{z_1 - z_2} \qquad (A17)$$

and $F(\psi, k)$ is an incomplete elliptic function of the first kind.[19-21]

The next step is to use eq A16 to obtain Fourier expansions in α_v for trigonometric functions of the polar angle θ. The most convenient approach involves the use of Jacobian elliptic functions $sn(u, k)$, $cn(u, k)$, etc.[19-21] Note first that the above integrals over z can be elegantly reduced to the formulas given above, by means of the substitution

$$\cos\theta = z = z_1 - (z_1 - z_2)sn^2(u, k) \qquad (A18)$$

together with the properties of the elliptic functions $sn(u, k)$, $cn(u, k)$, and $dn(u, k)$[19-21] and the identities

$$u = F(\psi, k) = 2\alpha_v K(k)/\pi \qquad (A19)$$

where the latter arise from the combination of eqs A12 and A16.

The function $sn(u, k)$ itself has the known Fourier series

$$sn(u, k) = \frac{2\pi}{K} \sum_{m=0}^{\infty} \frac{q^{m+1/2}}{1 - q^{2m+1}} \sin(2m + 1)\frac{\pi u}{2K(k)} \qquad (A20)$$

where

$$q = \exp[-\pi K(k')/K(k)], \quad k' = \sqrt{1 - k^2} \qquad (A21)$$

and the argument that follows extends the derivation of this result given by Whittaker and Watson.[23] The essential points are that $sn(u, k)$ is doubly periodic in the complex variable u, with periods $4K(k)$ and $2iK'(k)$, where $K'(k) = K(\sqrt{1 - k^2})$, and that $sn(u, k)$ has poles at $iK'(k)$ and $iK'(k) + 2K(k)$ [mod $4K(k)$, $2iK'(k)$], around which it varies as[23]

$$sn(u + iK') = -sn(u + 2K + iK') = \frac{1}{ku}\left[1 + \frac{1 + k^2}{6}u^2 + O(u^4)\right] \qquad (A22)$$

The dependence of $sn(u, k)$, $K(k)$, and $K'(k)$ on k is dropped in eq A22 and subsequent equations for notational convenience. The aim is to obtain a Fourier series for powers of $sn(u)$, which are expressed in the form

$$sn^k(u) = \sum_{v=-\infty}^{\infty} f_v^{(k)} e^{-iv u\pi/2K} \qquad (A23)$$

in which case the above properties of $sn(u)$ allow the coefficients

$$f_v^{(k)} = \frac{1}{4K} \int_{-2K}^{2K} sn^k(u) \, e^{-iv u\pi/2K} \, du \qquad (A24)$$

to be evaluated by the residue theorem. The contour is taken around the unit cell, with corners $-2K$, $2K$, $2K + 2iK'$, and $-2K + 2iK'$ slightly displaced to the right in order to enclose the pole at $2K + iK'$. The periodicity of $sn(u)$ ensures that the first and third segments of the contour integral differ by a factor $-q^v$, while the second and fourth segments cancel. Hence, by the residue theorem[24]

$$(1 - q^v) \int_{-2K}^{2K} sn^k(u) \, e^{iv u\pi/2K} \, du =$$
$$2\pi i[R^{(k)}(iK') + R^{(k)}(2K + iK')] \quad (A25)$$

where $R^{(k)}(iK')$, etc., denotes the residue at a kth-order pole. One finds from eq A22 for the specific cases $k = 2$ and $k = 4$ that

$$R^{(2)}(iK') = (-1)^v R^{(2)}(2K + iK') = \frac{iv\pi}{2k^2 K} q^{v/2} \quad (A26)$$

$$R^{(4)}(iK') = (-1)^v R^{(4)}(2K + iK') =$$
$$\frac{iv\pi}{12k^4 K} q^{v/2}\left[4(1 + k^2) - \frac{v^2\pi^2}{4K^2}\right] \quad (A27)$$

The factors $(-1)^v$ in eqs A26 and A27 ensure that $f_v^{(2)}$ and $f_v^{(4)}$ vanish for odd v, while the factor $v(q^{v/2} - q^{-v/2})$ implied by eqs A25−A27 means that $f_v^{(k)} = f_{-v}^{(k)}$ for $v \neq 0$ and $k = 2$ or 4. Consequently, $sn^2(u, k)$ and $sn^4(u, k)$ have the following cosine series in the angle $a_v = u\pi/2K$

$$sn^2(u, k) = \sum_{\mu=0}^{\infty} A_{2\mu}^{(2)}(k) \cos 2\mu\alpha \qquad (A28)$$

$$sn^4(u, k) = \sum_{\mu=0}^{\infty} A_{2\mu}^{(4)}(k) \cos 2\mu\alpha \qquad (A29)$$

where

$$A_{2\mu}^{(2)}(k) = \frac{2\pi^2}{k^2 K^2(k)} \frac{\mu}{q^\mu - q^{-\mu}}, \quad \mu \neq 0 \qquad (A30)$$

$$A_{2\mu}^{(4)}(k) = \frac{\pi^2}{3k^4 K^2(k)}\left[4(1 + k^2) - \frac{\mu^2\pi^2}{K^2}\right]\frac{\mu}{q^\mu - q^{-\mu}}, \quad \mu \neq 0 \qquad (A31)$$

The coefficients $A_0^{(2)}$ and $A_0^{(4)}$, which are undetermined by the above argument, may be obtained by direct integration.[19]

$$A_0^{(2)}(k) = \frac{1}{K} \int_0^K sn^2(u) \, du = \frac{1}{k^2 K(k)}[K(k) - E(k)] \quad (A32)$$

$$A_0^{(4)}(k) = \frac{1}{K} \int_0^K sn^4(u) \, du = \frac{1}{3k^4 K(k)}[(2 + k^2)K(k) -$$
$$2(1 + k^2)E(k)] \quad (A33)$$

The practical consequence of these results, for the present theory, is that

$$\sin^2\theta = \sum_{\mu=0}^{\infty} C_{2\mu}(\epsilon) \cos 2\mu\alpha \qquad (A34)$$

where $\epsilon = E/B$ and

Scaling Rules for Resonance Dynamics

J. Phys. Chem. A, Vol. 105, No. 12, 2001 **2841**

$$C_0(\epsilon) = (1 - z_1^2) + 2z_1(z_1 - z_2)A_0^{(2)}(k) - (z_1 - z_2)^2 A_0^{(4)}(k) \tag{A35}$$

$$C_{2\mu}(\epsilon) = 2z_1(z_1 - z_2)A_{2\mu}^{(2)}(k) - (z_1 - z_2)^2 A_{2\mu}^{(4)}(k), \quad \mu \neq 0 \tag{A36}$$

Equations A18 and A30−A33 have been used to obtain these results. Expressions for k, z_1, and z_2 in terms of the reduced energy ϵ are given for $m = 0$ in the following section. Equations A34−A36 also apply to nonzero angular momenta m, provided that the roots $\{z_i\}$ and hence k are derived from a suitably modified version of eq A9.

A.3. Explicit Results. To make the theory explicit, the working formulas may be expressed as functions of the reduced energy, $\epsilon = E/B$. Different expressions apply for $\epsilon < 1$ and $\epsilon > 1$, because of the changes in assigned z_i values given by eq A13. Useful limiting expressions for the Fourier coefficients, $C_{2\mu}(\epsilon)$, may also be obtained with the help of the following series:[19−21]

$$K(k) = \frac{\pi}{2}\left(1 + \frac{1}{4}k^2 + \frac{9}{64}k^4 + \frac{25}{256}k^6 + \frac{1225}{16384}k^8 + ...\right) \tag{A37}$$

$$E(k) = \frac{\pi}{2}\left(1 - \frac{1}{4}k^2 - \frac{3}{64}k^4 - \frac{5}{256}k^6 - \frac{175}{16384}k^8 + ...\right) \tag{A38}$$

$$q(k) = \frac{k^2}{16}\left[1 + 2\left(\frac{k}{4}\right)^2 + 15\left(\frac{k}{4}\right)^4 + 150\left(\frac{k}{4}\right)^6 + ...\right]^4 \tag{A39}$$

Below the Barrier Case: $\epsilon < 1$. The following identities apply at energies below the barrier

$$(z_1, z_2, z_3) = (1, 1 - 2\epsilon, -1) \tag{A40}$$

$$k^2 = \epsilon \tag{A41}$$

$$v + 1 = \frac{4\sqrt{2IB}}{\pi\hbar}[E(\epsilon^{1/2}) - (1 - \epsilon)K(\epsilon^{1/2})] \tag{A42}$$

$$\left(\frac{\partial E}{\partial v}\right)_m = \hbar\omega_b = \frac{\pi\hbar}{2}\sqrt{\frac{B}{2I}}\frac{1}{K(\epsilon^{1/2})} \tag{A43}$$

Similarly, it follows from eq A15 that

$$\sin^2\theta = 1 - [1 - 2\epsilon\,\mathrm{sn}^2(u)]^2 = 4\epsilon[\mathrm{sn}^2(u) - \epsilon\,\mathrm{sn}^4(u)] \tag{A44}$$

from which, with the help of eqs A28−A36,

$$C_0 \simeq 2\epsilon - \frac{5}{4}\epsilon^2 - \frac{1}{8}\epsilon^3 \tag{A45}$$

$$C_2 \simeq -2\epsilon + 2\epsilon^2 + \frac{19}{28}\epsilon^3 \tag{A46}$$

$$C_4 \simeq -\frac{3}{4}\epsilon^2 + \frac{1}{8}\epsilon^3 + \frac{5}{64}\epsilon^4 \tag{A47}$$

$$C_6 \simeq -\frac{19}{128}\epsilon^3 - \frac{1}{16}\epsilon^4 - \frac{271}{8192}\epsilon^5 \tag{A48}$$

Above barrier case: $\epsilon > 1$. The corresponding expressions at energies above the barrier are as follows:

$$(z_1, z_2, z_3) = (1, -1, 1 - 2\epsilon) \tag{A49}$$

$$k^2 = \epsilon^{-1} \tag{A50}$$

$$v + 1 = \frac{4\sqrt{2IB}}{\pi\hbar}\epsilon^{1/2}E(\epsilon^{-1/2}) \tag{A51}$$

$$\left(\frac{\partial E}{\partial v}\right)_m = \hbar\omega_b = \frac{\pi\hbar}{2}\sqrt{\frac{B}{2I}}\frac{\epsilon^{1/2}}{K(\epsilon^{-1/2})} \tag{A52}$$

$$\sin^2\theta = 1 - [1 - 2\mathrm{sn}^2(u)]^2 = 4[\mathrm{sn}^2(u) - \mathrm{sn}^4(u)] \tag{A53}$$

$$C_0 \simeq \frac{1}{2} - \frac{3}{256}\epsilon^{-2} - \frac{3}{256}\epsilon^{-3} \tag{A54}$$

$$C_2 \simeq \frac{1}{8}\epsilon^{-1} + \frac{7}{48}\epsilon^{-2} + \frac{39}{1024}\epsilon^{-3} \tag{A55}$$

$$C_4 \simeq -\frac{1}{2} + \frac{1}{32}\epsilon^{-2} + \frac{1}{32}\epsilon^{-3} \tag{A56}$$

$$C_6 \simeq -\frac{1}{8}\epsilon^{-1} - \frac{1}{16}\epsilon^{-2} - \frac{73}{2048}\epsilon^{-3} \tag{A57}$$

References and Notes

(1) McCoy, A. B.; Sibert, E. L., III. *J. Chem. Phys.* **1996**, *105*, 459.
(2) Joyeux, M. *J. Chem. Phys.* **1998**, *109*, 2111.
(3) Iachello, F.; Levine, R. D. *Algebraic Theory of Molecules*; Oxford University Press: New York, 1995.
(4) Sako, T.; Yamanouchi, K. *Chem. Phys. Lett.* **1997**, *264*, 403.
(5) Kellman, M. E. *Annu. Rev. Phys. Chem.* **1995**, *46*, 395.
(6) Perez Bernal, F.; Bijker, R.; Frank, A.; Lemus, R.; Arias, J. M. *Chem. Phys. Lett.* **1996**, *258*, 301.
(7) Jacobson, M. P. Ph.D. Thesis, Massachusetts Institute of Technology, Cambridge, MA, 1999.
(8) El Idrissi, M. I.; Liévin, J.; Campargue, A.; Herman, M. *J. Chem. Phys.* **1999**, *110*, 2074.
(9) Jacobson, M. P.; Child, M. S. *J. Chem. Phys.* **2001**, *114*, 250.
(10) Jacobson, M. P.; Child, M. S. *J. Chem. Phys.* **2001**, *114*, 262.
(11) Ishikawa, H.; Field, R. W.; Farantos, S. C.; Joyeux, M.; Koput, J.; Beck, C.; Schinke, R. S. *Annu. Rev. Phys. Chem.* **1999**, *50*, 443.
(12) Dixon, R. N. *Trans. Faraday Soc.* **1964**, *60*, 1363.
(13) Child, M. S. *Semiclassical mechanics with molecular applications*; Oxford University Press: Oxford, U.K., 1994.
(14) Heisenberg, W. *Zeit. Phys.* **1925**, *33*, 879.
(15) Lichtenberg, A. J.; Lieberman, M. A. *Regular and stochastic motion*; Springer-Verlag: New York, 1983.
(16) Tabor, M. *Chaos and integrability in nonlinear dynamics*; Wiley-Interscience: New York, 1989.
(17) Fried, L. E.; Ezra, G. S. *J. Chem. Phys.* **1987**, *86*, 6270.
(18) Kellman, M. E. *J. Chem. Phys.* **1990**, *93*, 6630.
(19) Byrd, P. F.; Friedman, M. D. *Handbook of elliptic integrals for engineers and physicists*; Springer-Verlag: New York, 1954.
(20) Gradsteyn, I. S.; Ryzhik, I. M. *Tables of integrals, series and products*, 5th ed.; Academic Press: New York, 1994.
(21) Abramowitz, M.; Stegun, I. A. *Handbook of mathematical functions*; Dover: New York, 1965.
(22) Goldstein, H. *Classical mechanics,* 2nd ed.; Addison-Wesley: New York, 1980.
(23) Whittaker, E. T.; Watson, G. N. *A course in modern analysis*, 4th ed.; Cambridge University Press: Cambridge, U.K., 1952.
(24) Arfken, G. *Mathematical methods for physicists*, 3rd ed.; Academic Press: New York, 1985.